Simulating transport of non-Chernobyl ^{137}Cs and ^{90}Sr in the North Atlantic–Arctic region

Yongqi Gao [a], **Helge Drange**[a, b, c], **Mats Bentsen**[a, b] **and Ola M. Johannessen**[a, c]

[a] Nansen Environmental and Remote Sensing Center, Bergen, Norway
[b] Bjerknes Centre for Climate Research, Bergen, Norway
[c] Geophysical Institute, University of Bergen, Bergen, Norway

Abstract

The spatial and temporal distributions of the anthropogenic radionuclides ^{137}Cs and ^{90}Sr, originating from nuclear bomb testing and the Sellafield reprocessing plants in the Irish Sea, are simulated using a global version of the Miami Isopycnic Coordinate Ocean Model (MICOM). The physical model is forced with daily atmospheric re-analysed fields for the period 1950 to present. Comparison of temporal evolution of observed and simulated concentrations of ^{137}Cs have been conducted for the regions east of Scotland, west of central Norway and at the entrance of the Barents Sea. It follows that the radionuclides from the Sellafield discharge reach the Barents Sea region after 4–5 years, in accordance with observations. The simulation provides a detailed distribution and evolution of the radionuclides over the integration time. For the Atlantic waters off the coast of Norway and in the southern Barents Sea, the atmospheric fallout dominates over the Sellafield release up to the mid 1960s and from the early 1990s, whereas Sellafield is the main source for the two radionuclides in the 1970s and 1980s. It is furthermore argued that model systems like the one presented here can be used for future prediction of radioactive contaminations in the Nordic Seas and the Arctic Ocean, for instance under various global warming scenarios.

Author Keywords: Sellafield release; Atmospheric fallout; Nordic Seas; Arctic Ocean; Transport

1. Introduction

A scientifically based description, understanding, quantification and potential prediction of the spatial distribution, temporal evolution and biogeochemical consequences of human-generated contamination of the environment require integrated use of observations and numerical modelling. Here a 3D numerical ocean general circulation model (OGCM) is used to demonstrate the usefulness, and also to point towards the limitations, of simulating pathways and levels of trace compounds in the ocean environment. The trace compounds used in the study are the anthropogenic radionuclides ^{137}Cs and ^{90}Sr originating from nuclear bomb testing and the Sellafield release to the Irish Sea.

The model system used in this work has been validated against observed chlorofluorocarbon (CCl_3F and CCl_2F_2) distributions in the North Atlantic Ocean for the period 1930 to present ([Gao et al., in press]), focusing on multi-annual to decadal scale ventilation and water mass transformation processes in the region. In addition, mass transports in and out of the Nordic Seas region have been validated based on observations and observational based estimates for the last 40 years ([Nilsen et al., in press]). Both studies show that the model system is able to describe most of the key observed quantities in a fairly

realistic manner. It is therefore believed that the model system is a potentially useful tool in simulating the advective transport and dispersive mixing of radionuclides that behave conservatively in sea water.

The objective of the study is to use ^{137}Cs and ^{90}Sr to simulate the transport and dispersion of coastal pollution from Europe to the Arctic Ocean (e.g., [Dahlgaard, 1995 and Nies et al., 1998]), and to assess the relative contributions from the nuclear bomb testing and the Sellafield release in the region. The release from the Chernobyl accident in 1986 is not included in the present integration because of uncertainties in the temporal–spatial source function. The Chernobyl release will be addressed in another paper.

The simulation differs from the large scale OGCM simulation by [Nies et al., 1998] in the following ways: a fully on-line instead of off-line integration procedure is adopted; the model is forced with synoptic (i.e. daily) atmospheric fields instead of climatological (i.e. monthly mean) forcing fields; a truly global OGCM with a horizontally stretched grid system is used instead of a regional North Atlantic–Arctic model set-up; both atmospheric fallout and the Sellafield discharge are simulated in contrast to the Sellafield release only; and the integration time period is 1950–1999 compared to 1965–1995.

The paper is organized as follows: a description of the model system is provided in Section 2. In Section 3, a brief overview of the ocean circulation in the Atlantic–Arctic Ocean is given, together with the observed distribution of the ^{137}Cs and ^{90}Sr radionuclides. The radionuclides simulation is described in Section 4. The obtained results are given in Section 5, and the paper is summarized in Section 6.

2. Model description

The model system applied in this study is the OGCM Miami Isopycnic Coordinate Ocean Model (MICOM) ([Bleck et al., 1992]), fully coupled to a sea-ice module consisting of the [Hibler, 1979] rheology in the implementation of [Harder, 1996], and the thermodynamics of [Drange and Simonsen, 1996].

The model has 23 layers with fixed potential densities, and an uppermost mixed layer (ML) with temporal and spatial varying density. The specified potential densities of the sub-surface layers were chosen to ensure a realistic representation of the major water masses in the North Atlantic–Nordic Sea region. The densities of the isopycnic layers (in σ_0-units) are 24.12, 24.70, 25.28, 25.77, 26.18, 26.52, 26.80, 27.03, 27.22, 27.38, 27.52, 27.63, 27.71, 27.77, 27.82, 27.86, 27.90, 27.94, 27.98, 28.01, 28.04, 28.07 and 28.10. In the horizontal, the model is configured with a local orthogonal grid mesh with one pole over North America and one pole over western part of Asia ([Bentsen et al., 1999]), yielding a grid-spacing of about 90–120 km in the North Atlantic–Nordic Seas region.

The vertically homogeneous ML utilises the [Gaspar, 1988] bulk parameterization for the dissipation of turbulent kinetic energy, and has temperature, salinity and layer thickness as the prognostic variables. In the isopycnic layers below the ML, temperature and layer thickness are the prognostic variables, whereas salinity is diagnostically determined by means of the simplified equation of state of [Friedrich and Levitus, 1972]. The bathymetry is computed as the arithmetic-mean value based on the ETOPO-5 data base (Data Announcement 88-MGG-02, Digital relief of the Surface of the Earth, NOAA, National Geophysical Data Center, Boulder, Colorado, 1988).

The continuity, momentum and tracer equations are discretised on an Arakawa C-grid stencil ([Arakawa

and Lamb, 1977]). The diffusive velocities (diffusivities divided by the size of the grid cell) for layer interface diffusion, momentum dissipation, and tracer dispersion are 0.015, 0.015 and 0.005 m s^{-1}, respectively. A flux corrected transport scheme ([Zalesak, 1979 and Smolarkiewicz and Clark, 1986]) is used to advect the model layer thickness and the tracer quantities.

The diapycnal mixing coefficient K_d (m^2 s^{-1}) is parameterized according to the [Gargett, 1984] expression K_d=3×10^{-7}/N, where N (s^{-1}) is the Brunt-Väisälä frequency. The numerical implementation of the diapycnal mixing follows the scheme of [McDougall and Dewar, 1998].

The model was initialized by the January [Levitus and Boyer, 1994] and [Levitus et al., 1994] climatological temperature and salinity fields, respectively, a 2 m thick sea-ice cover based on climatological sea-ice extent, and an ocean at rest. The model was first spun-up for 180 years with monthly mean atmospheric forcing fields derived from the NCEP/NCAR reanalysis ([Kalnay et al., 1996]). In this spin-up, both sea surface salinity (SSS) and sea surface temperature (SST) was relaxed towards monthly mean surface climatology. The relaxation was carried out by applying fluxes of heat and salt proportional to the SSS and SST differences between model and climatology, respectively, with an *e*-folding time scale of 30 days for a ML of 50 m or less, decreasing linearly with thicker ML depths. The spin-up was then continued with daily NCEP/NCAR forcing, repeating the period 1974–1978 twice. Only salinity relaxation was applied in these two integrations, and the deduced salinity adjustment flux was stored from the latter integration to produce seasonal averaged restoring fluxes for salt. The period 1974–1978 was chosen because of the relatively neutral North Atlantic Oscillation (NAO; [Hurrell, 1995]) conditions of these years (see below). Finally, the model was integrated with daily forcing for the period 1948–1999 with no relaxation but with the diagnosed restoring fluxes for salt.

2.1. The tracer module

The transport and mixing of the radionuclides follow the equation ([Bleck et al., 1992])

$$\frac{\partial}{\partial t}\left(\frac{\partial p}{\partial s}C\right) + \nabla_s\left(\vec{v}\,\frac{\partial p}{\partial s}C\right) + \underbrace{\frac{\partial}{\partial s}\left(\dot{s}\frac{\partial p}{\partial s}C\right)}_{\text{mass transfer}} = \underbrace{\nabla_s\left(v\frac{\partial p}{\partial s}\nabla_s C\right)}_{\text{diffusion}} + \underbrace{\delta_C}_{\text{source/sink}} - \underbrace{\lambda C}_{\text{decay}}$$

(1)

Here p is the interface pressure of the isopycnals, C is the concentrations of the tracers, $\vec{v}$ is the isopycnal velocity, s is the vertical coordinate, v is the diffusive velocity for the tracers, and λ denotes the decay of C. Both ^{137}Cs and ^{90}Sr are soluble in sea water and can be considered as passive tracers with a half-life of 30.1 and 29 years, respectively.

3. Observed distribution of water masses and radionuclides

The ocean circulation in the region of interest is complex and is characterized by warm and saline surface Atlantic water (AW) flowing through the Denmark Strait, passing the ridge between Iceland and the Faroes, and entering east of the Faroes ([Hansen and Østerhus, 2000]). Observational based estimates of the transport of AW through these openings are 1 Sv ([Hansen and Østerhus, 2000]), 3.3 Sv ([Hansen and Østerhus, 2000]) and 4.3 Sv ([Turrell et al., 2002]), respectively (1 Sv=10^6 m^3 s^{-1}). The AW continues northward along the Norwegian coast as the Norwegian Atlantic Current (NAC). One branch of

the AW enters the Barents Sea (2.3 Sv; [Ingvaldsen et al., 2002]), whereas the remaining AW continues to the Fram Strait as the West Spitsbergen Current (WSC). Here a fraction of the AW subducts and enters the Arctic Ocean, whereas the rest recirculates and flows southward.

The mean simulated surface current field from our model study in the Atlantic–Arctic region is displayed in Fig. 1. The circulation field is, in general, in accordance with observations. The most pronounced exception is the too northerly separation of the Gulf Stream off the North American coast. This is a classical problem for OGCMs; a properly resolved Gulf Stream requires a horizontal resolution one order of magnitude higher than in the present integration ([Bleck et al., 1995]).
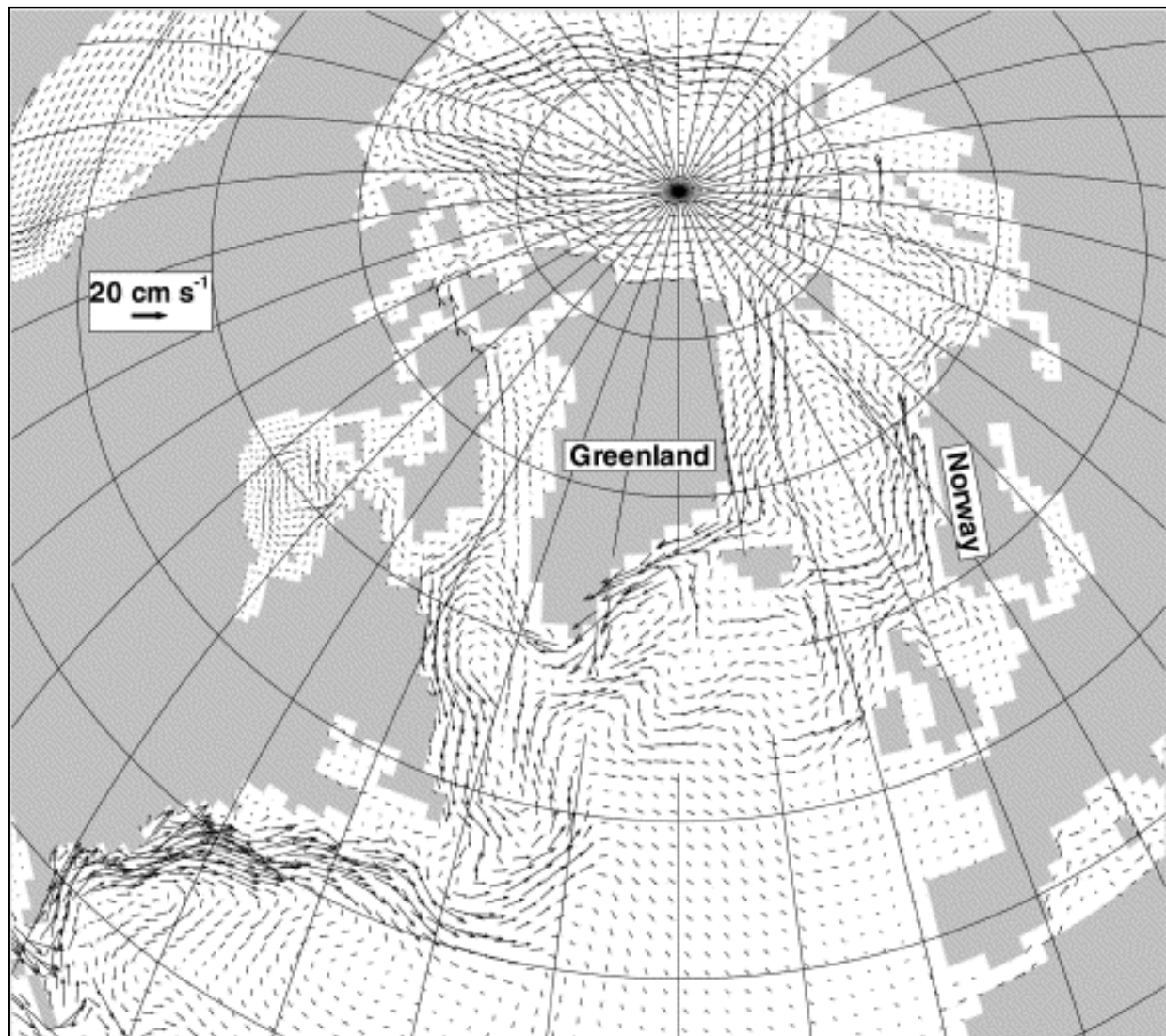
Fig. 1. The simulated mean circulation field in the upper 100 m of the water column for the period 1950–1999.

Furthermore, the general surface ocean circulation in the Arctic Ocean is dominated by the Beaufort Gyre and the Transpolar Drift (TPD). As already stated, volume exchanges between the Arctic Ocean and the North Atlantic take place via the Barents Sea and through the Fram Strait. The cold and fresh polar water leaves the Arctic with the East Greenland Current (EGC) on the western side of the Fram Strait. This water continues southward along the coast of Greenland. Most of the polar water flows through the Denmark Strait and enters the sub-polar gyre. A branch of the cold and fresh Arctic water flows eastward north of the Denmark Strait and is trapped in the cyclonically directed circulation in the Nordic Seas.

The pathway of the soluble radionuclides ^{137}Cs and ^{90}Sr from Sellafield to the Arctic has been summarized by [Kershaw and Baxter, 1995] (see Fig. 2). Initially the tracer is carried northward from the Irish Sea as a plume-like structure via the North Channel, and it then flows along the coast of Scotland into the North Sea. The tracer is transported northward before branching off northern Norway: One branch passes eastwards into the Barents Sea; the other passes through the Fram Strait with the WSC. The main surface water return flow occurs with the EGC. In case the tracer is mixed into sub-surface waters, the return flow will also include the Denmark Strait overflow, the overflow across the Iceland–Faroe Ridge and the Faroe–Bank Channel overflow ([Hansen and Østerhus, 2000]).
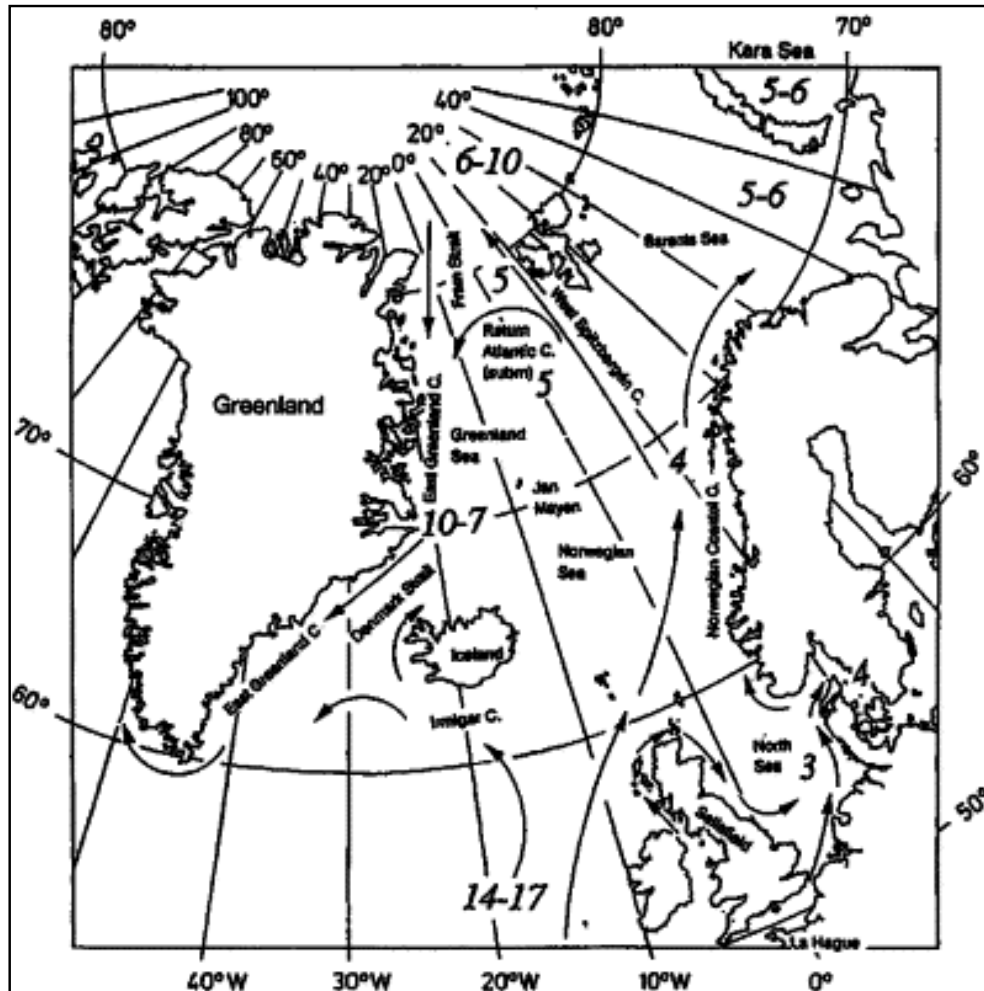
Fig. 2. Estimated pathway and transit time (yr) of the Sellafield signal, adapted from [Dahlgaard, 1995].

Fig. 2 also provides estimated transit times for the Sellafleld release. It follows that the signal enters the Barents Sea after about 4 years. In the Fram Strait, the transit time is about 5 years for the AW and 6–10 years for the southward flowing Arctic waters. After additional 2 years, the Sellafield signal passes the Denmark Strait, and continues cyclonically along the periphery of the sub-polar gyre. It is further speculated that a part of the signal from the sub-polar gyre re-enters the northward flowing AW after a total transit time of 14–17 years.

4. The radionuclides simulation

Nuclear bomb testing, the Chernobyl accident and release from the European reprocessing plants Sellafield (the UK) and Cap de La Hague (France) are the most important sources for the radionuclides in

the North Atlantic–Arctic region ([Nies et al., 1998]). The time evolution of ^{137}Cs and ^{90}Sr from the Sellafield release, from the nuclear bomb testing and from the Chernobyl accident in 1986 over Denmark (S. Nielsen, personal communication, 2001) is shown in Fig. 3. The atmospheric fallout provides the present background concentration of the surface and sub-surface waters of the region, while the Sellafield discharge is one of the major sources of radioactive contamination in the Arctic Ocean since the 1970s ([Strand et al., 1996]). The Sellafield signal has been observed over the last two decades, making model-evaluation of in particular ^{137}Cs distributions possible.
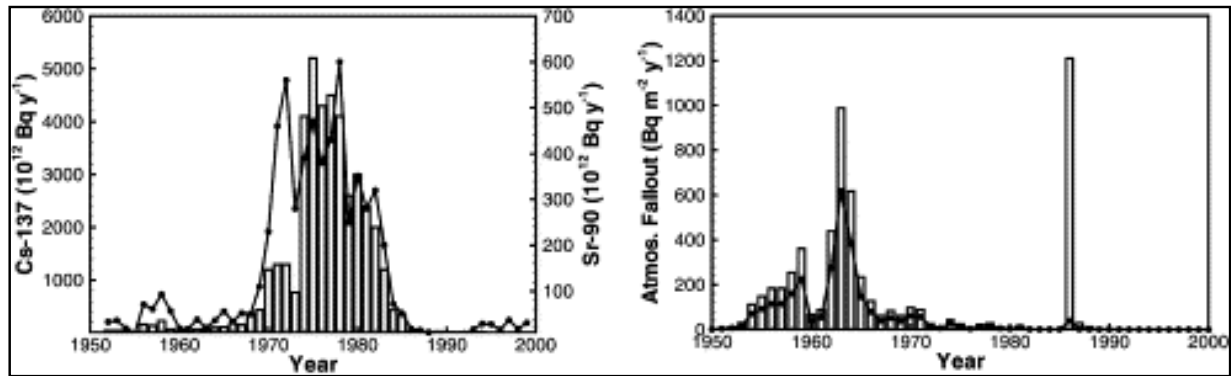
Fig. 3. The time evolution of ^{137}Cs (bars) and ^{90}Sr (line) from (a) the Sellafield release (unit: 10^{12} Bq y^{-1}) and (b) the atmospheric fallout (unit: Bq m^{-2} y^{-1}) over Denmark. (S. Nielsen, personal communication, 2001).

The latitudinal distribution of the atmospheric ^{90}Sr deposition ([UNSCEAR, 1982]; see Fig. 4) makes it feasible to construct the latitudinal distribution of the atmospheric fallout of ^{137}Cs, with the fallout of ^{137}Cs a factor 1.6 higher than that of ^{90}Sr ([Strand et al., 1998]). A total of four tracers are included in the simulation; the atmospheric fallout of ^{137}Cs and ^{90}Sr, and the Sellafleld discharge of ^{137}Cs and ^{90}Sr. The Chernobyl release in 1986, seen as the isolated peak in the atmospheric fallout in Fig. 3b, is not included in the present integration. The initial fields of all of the radionuclides are set to zero. The simulation starts in 1950 and ends in 1999.
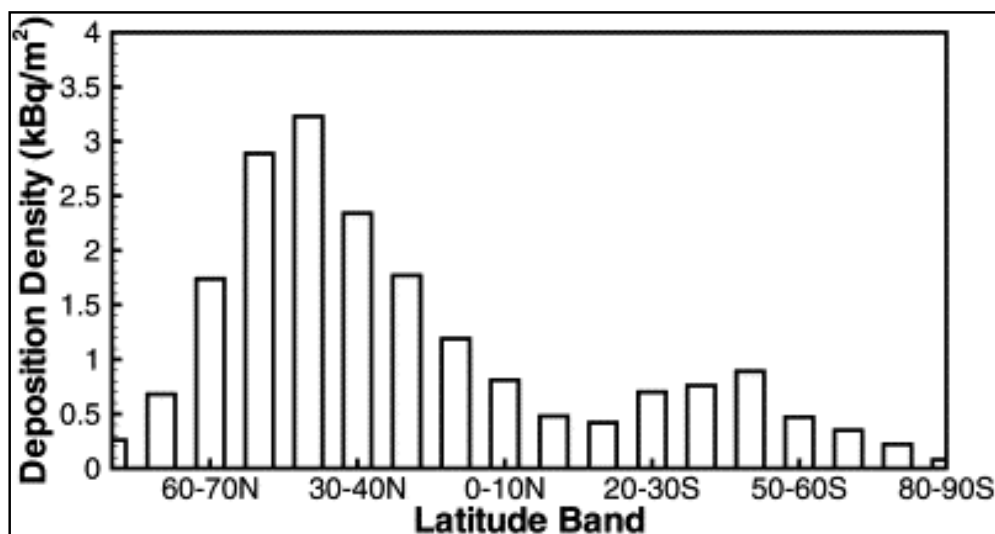

Fig. 4. The atmospheric deposition of ^{90}Sr (kBq m^{-2}) vs. latitude ([UNSCEAR, 1982]).

5. Result

Before extending northward with the NAC, the simulated Sellafield radionuclides circulate cyclonically in the North Sea (see Fig. 1 and Fig. 5). One branch enters the Barents Sea, and one branch heads towards the Fram Strait following the WSC. The simulated pathway of the Sellafield release to the Barents Sea is in general agreement with observations ([Kershaw and Baxter, 1995], and Fig. 2). In the Barents Sea, the Sellafield signal spreads towards north-east, and one branch enters the northern Kara Sea. The simulated Sellafield signal has passed the Denmark Strait by the EGC in year 1975 and is found in the Labrador Sea in the early 1980s. It should be noted that the simulated Sellafleld signal does not extend eastward of the Kara Sea, instead, the signal propagates westward following the Canadian Archipelago in the 1980s. It is also seen that the surface ^{137}Cs concentration is quickly decreasing in the late 1990s.
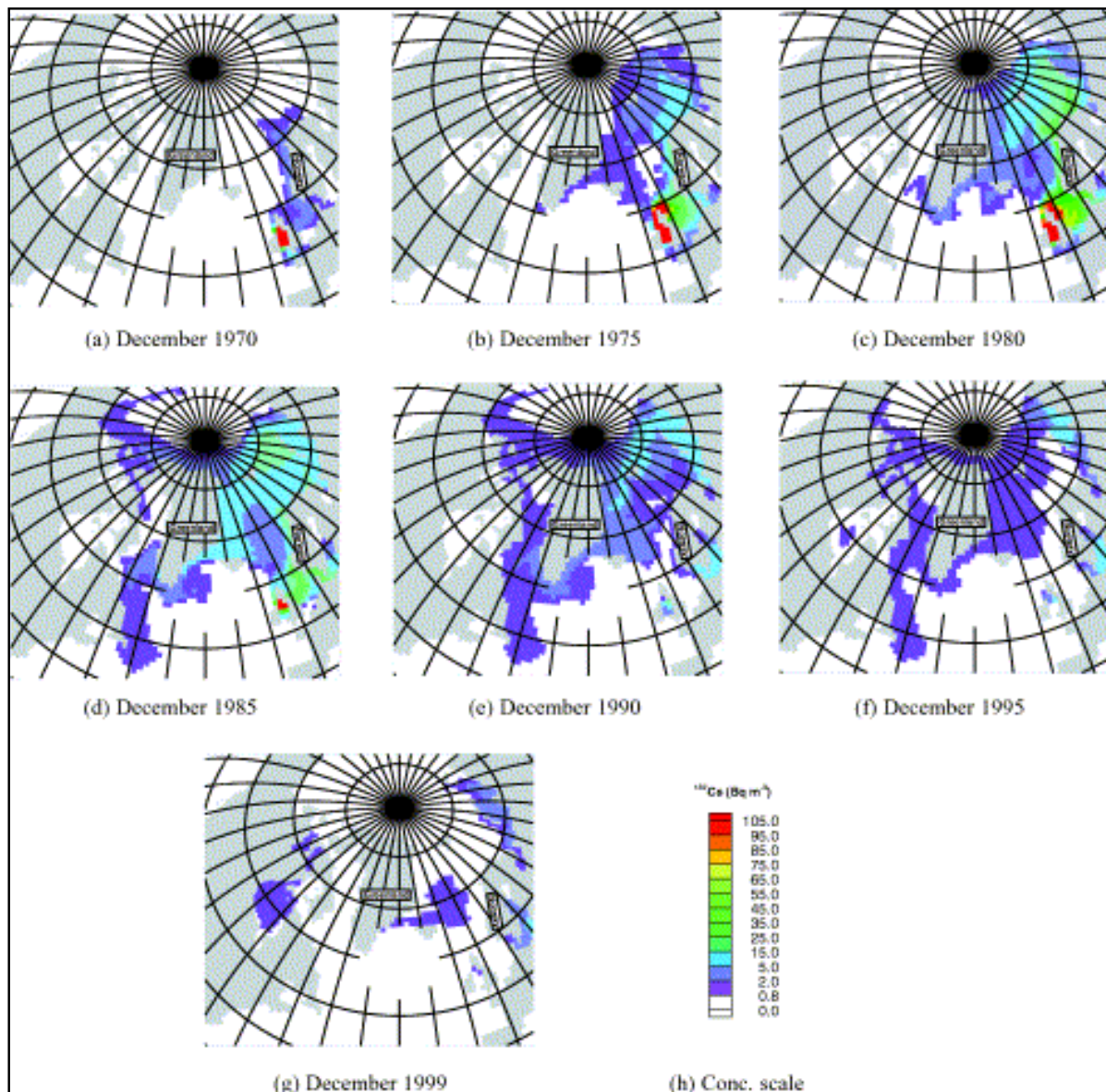

Fig. 5. Simulated surface distribution of ^{137}Cs (Bq m^{-3}) in December 1970 to December 1999 caused by the Sellafield release. Concentration scale in (h), with cut-off value of 1 Bq m^{-3}.

Fig. 6 and Fig. 7 display the evolution of the vertically integrated inventory of ^{137}Cs and the ratio of the vertically integrated inventory from Sellafield to that from atmospheric fallout, respectively. Generally, the inventory in the central Arctic Ocean is low due to the rather weak intrusion of the radioactive signal

from the AW. In the Barents Sea and west of Norway, the Sellafield contribution plays the dominant role in the inventory in the 1970s and 1980s. In the central Nordic Seas, the Sellafield source dominates the inventory from the mid 1980s.
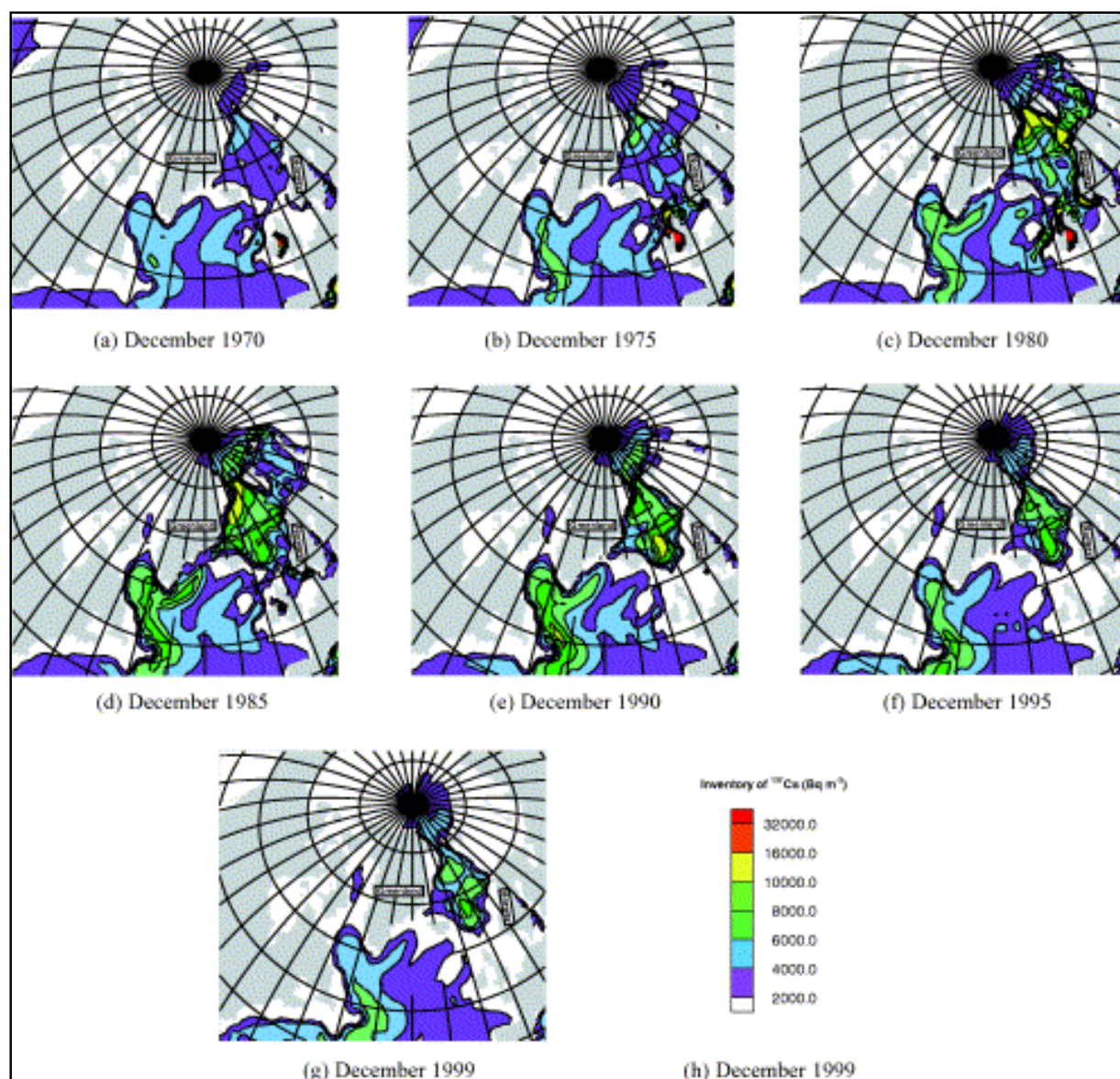

Fig. 6. Simulated vertically integrated inventory of ^{137}Cs (Bq m^{-2}) in December 1970 to December 1999 caused by the Sellafield release and atmospheric fallout. Inventory scale in (h), with a cut-off value of 2000 Bq m^{-2}.
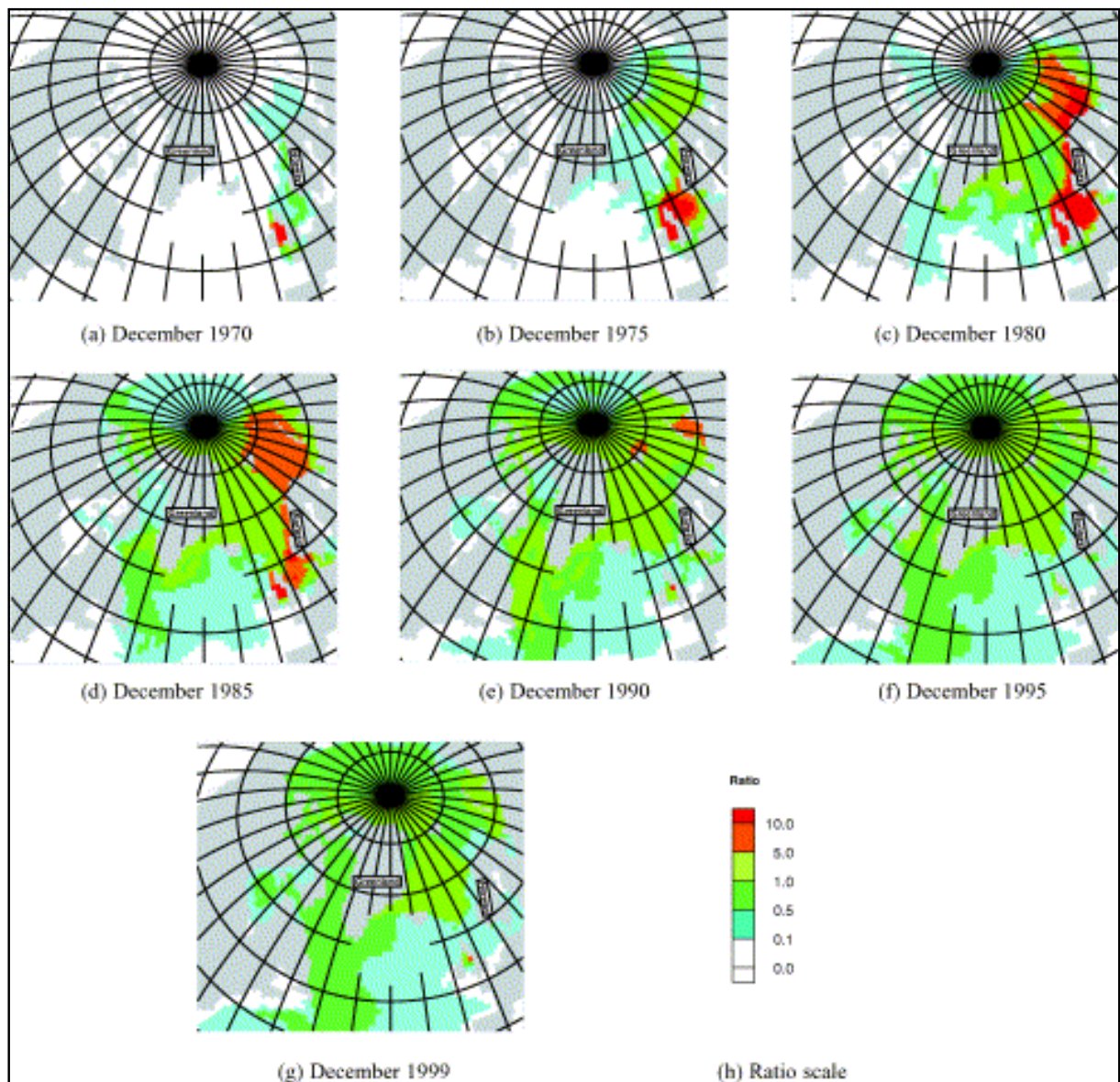
Fig. 7. Simulated ratio of the vertically integrated inventory of the Sellafield release to that of the atmospheric fallout in December 1970 to December 1999. Ratio scale in (h), with a cut-off value of 0.1.

The distribution of the Sellafield signal is closely associated with the simulated circulation field in the region. In Fig. 8, the circulation *anomalies* associated with years with high (1957, 61, 73, 75, 76, 81, 83, 84, 89, 90, 92, 93, 94, 95, 99) and low (1958, 60, 62, 63, 64, 65, 66, 68, 69, 70, 71, 77, 79, 87, 96) NAO-index ([Hurrell, 1995]) are displayed. The high and low NAO anomalies are associated with the most profound atmospheric winter time anomalies in the region ([Visbeck et al., in press]), and therefore illustrate the degree of long-term (i.e. multi-annual) variability in the surface circulation field. It should be mentioned that short-term variability occurring on time scales of days to months will far exceed the variability depicted in Fig. 8. The robust long-term changes, however, are expected to follow the changes in Fig. 8.
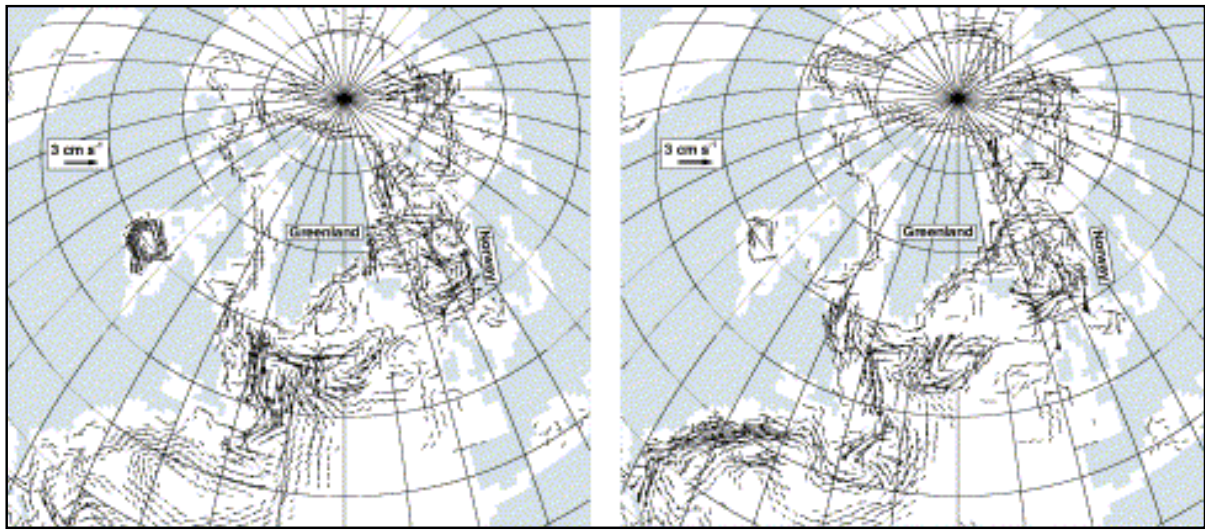
Fig. 8. The simulated surface circulation anomalies for high (a) and low (b) NAO indexes.

For high NAO-forcing (i.e. for fairly persistent and strong westerlies in the North Atlantic), there is an enhanced northward transport of water east of the Faroes and southward transport through the Denmark Strait (Fig. 8a). This result is in general accordance with observational based estimates ([Nilsen et al., in press]). There are also enhanced surface transports into the Barents Sea and of Arctic waters out of the Arctic Ocean through the Fram Strait. For years with low NAO-forcing, the anomalies oppositely mirror those of the high NAO-forcing closely (Fig. 8a).

The temporal variability of the simulated volume transports over the uppermost 100 m of the water column for some of the major openings in the Nordic Seas–Arctic region is provided in Fig. 9. The trend seen in these panels are in general agreement with the gradually increasing NAO-index over the time period from the early 1960s to the mid 1990s ([Hurrell, 1995]), and points toward the need for using synoptic rather than climatological forcing fields for tracer simulations.
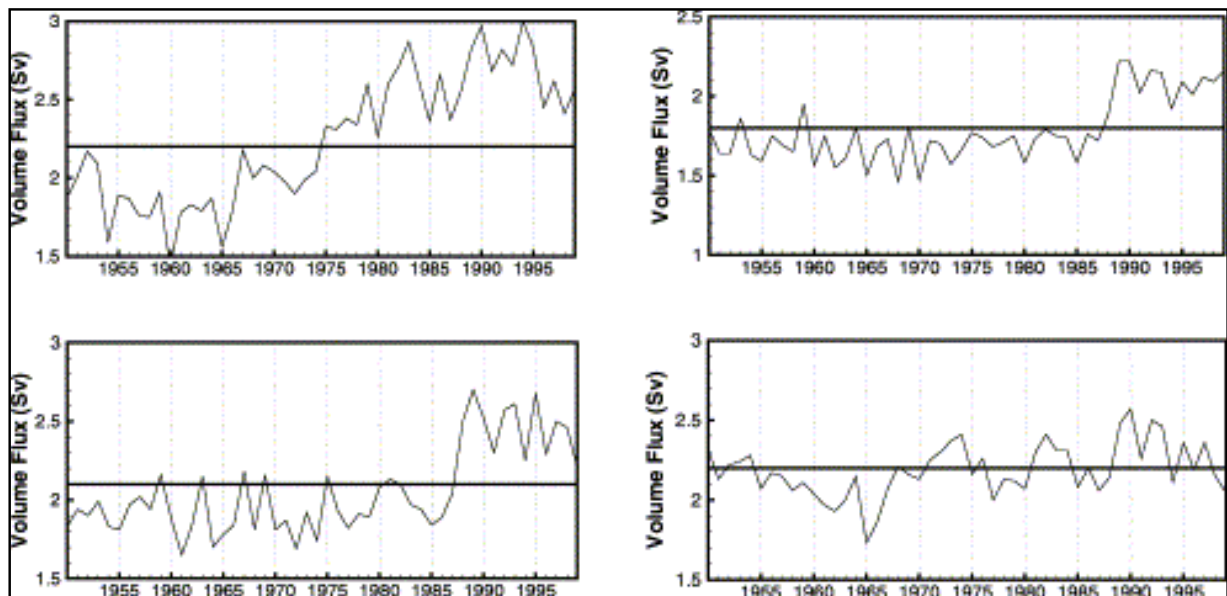

Fig. 9. Simulated time series of the volume transports (in Sv) over the upper 100 m for (a) the northward transport through the Faroe–Shetland Channel, (b) the northward transport through the Barents Opening, (c) the southward transport through the Farm Strait, and (d) the southward transport through the Denmark Strait. The thick solid lines indicate the averaged surface transport

over the period from 1950 to 1999 (2.2, 1.8, 2.1 and 2.2 Sv, respectively).

To qualitatively and quantitatively evaluate the simulated transport and mixing of the Sellafield discharge, time series of the observed and simulated surface ^{137}Cs concentration east of Scotland (57.0–57.5°N, 1.5–2.0°W), west of Norway (59–61°N, 3.5–5.0°E) and in the south-western Barents Sea region (71–72°N, 20–30°E) are shown in Fig. 10. The simulated ^{90}Sr signal is also shown in the figure. Superimposed on the panels, there is a histogram of the annual mean Sellafield discharge rates.
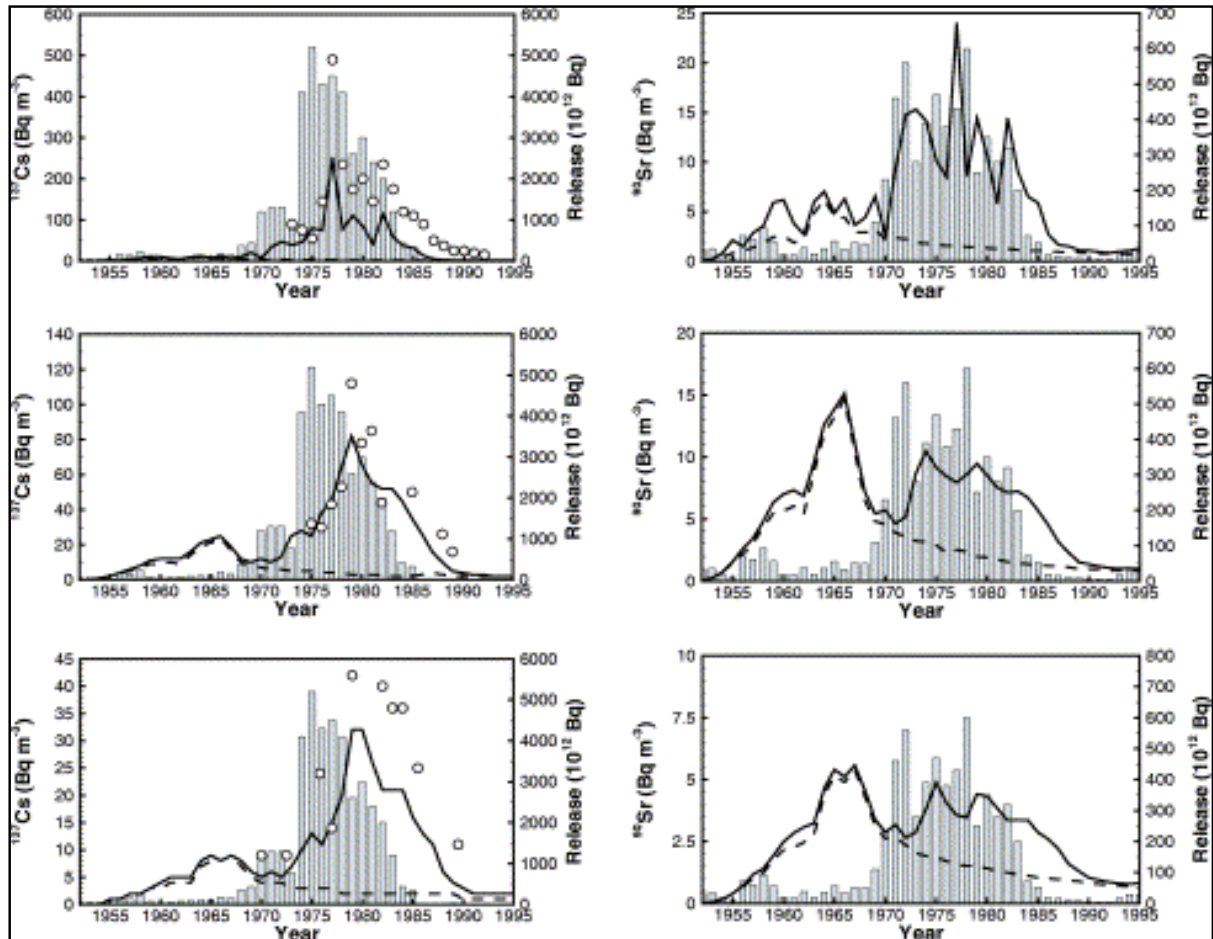

Fig. 10. Time series of the imposed Sellafield release rates of (10^{12} Bq y^{-1}; bars), the observed ^{137}Cs surface concentration (Bq m^{-3}) from [Kershaw and Baxter, 1995] in circles, and the simulated surface concentration for atmospheric fallout (dashed lines) and the sum of the Sellafield release and the atmospheric fallout (solid lines) for east of Scotland (upper row), west of Norway (mid row) and in the south-west Barents Sea region (lower row). ^{137}Cs to the left and ^{90}Sr to the right. Note the different concentration scales on the panels.

Clearly, the atmospheric fallout dominates the surface ^{137}Cs and ^{90}Sr distributions in mid 1960s in the three regions. However, from the late 1970s to the late 1980s, the Sellafield discharge heavily dominates the surface concentrations. For the last 5–10 years of the simulation, the surface concentrations of ^{137}Cs and ^{90}Sr are mainly governed by the atmospheric fallout.

The temporal and spatial evolution of the surface ^{137}Cs concentrations are in broad agreement with observations (Fig. 10a,c,e). However, the simulated surface ^{137}Cs concentrations are generally lower than the observed values. For instance, the maximum concentration in the Barents Sea is about 75% of the observed value. This finding, at least up to the Chernobyl accident in 1986, may indicate that the applied

model resolution is too coarse. It is also likely that reduced diapycnal and isopycnal mixing rates of a factor 2–4 would maintain higher peak tracer concentrations (cfr. [Gao et al., in press]).

Based on the simulated ^{137}Cs concentration fields, the time for the Sellafield release to reach eastern Scotland is 2 years, 4 years for western Norway and 4–5 years for southwestern Barents Sea. The transit time is here defined as the difference in time when the maximum concentration occurs in the specific region and when the maximum Sellafield release occurred. The simulated transit times are in accordance with earlier studies ([Kershaw and Baxter, 1995 and Livingston et al., 1984]; and Fig. 2).

6. Discussion and conclusion

The quality or realism of simulated tracer distributions is by necessity constrained by the simulated water mass transport and transformation rates. The classical way to validate an OGCM is to perform some base-line integrations, and thereafter compare the simulated fields (temperature, salinity, velocity, and derived parameters thereof) with observations. Based on this comparison, model parameters can be tuned, parameterization schemes changed or the numerics improved. In addition, inherent model deficiencies can be uncovered.

Unfortunately, the temporal–spatial distribution of hydrodynamic and dynamic in situ ocean observations are sparse. In addition, apparently realistic simulated hydrography can lead to erroneous current fields as demonstrated by e.g. [Toggweiler et al., 1989]. For this reason, validation of OGCMs based on well-documented tracer distributions with well-defined source functions (e.g., chlorofluorocarbons and natural and bomb-produced radiocarbon), in addition to the conventional hydrographic and transport validations, represent a powerful and cost-efficient OGCM validation strategy ([England and Holloway, 1998 and England and Maier-Reimer, 2001]).

A well-tested and validated numerical model system can be used to provide guidance of the short-term (days) to long-term (decadal) transport and spreading of trace compounds for prescribed source functions. This can be done by performing a series of integrations with the OGCM forced with atmospheric fields provided by an atmospheric forecast system with predictable skill of typically 4–6 days, by forcing a series of OGCM simulations with combinations of observed reanalysed fields available for the last 50 years (e.g., from the NCAR/NCEP re-analysis project, [Kalnay et al., 1996]) or, for a global warming scenario, by adopting forcing fields from a fully coupled climate model. For all types of experiments, the ensemble mean pathway and concentration level, together with statistics describing the spreading of the ensemble members, yield information about the likely spatial–temporal evolution of the tracers. These results are valuable as input for optimizing the observational strategy and to assess transit times and possible transport routes of the tracers.

In addition, the circulation field and water mass transformation rates from an OGCM can be used to identify possible source locations of various trace compounds based on isolated observations. The use of such an inverse modelling approach is a powerful tool for guiding an observational network to monitor the origin and the spatial–temporal evolution of the tracers.

In the model study of [Nies et al., 1998], monthly mean climatological forcing fields were used, yielding a simulated transport time from Sellafield to the Barents Sea of 6 years. In the simulation presented here, the corresponding time is 4–5 years, or approximately the transit time based on observations. The difference highlights the importance of using the more energetic synoptic forcing fields to drive the model. In addition, synoptic forcing fields will, in general, result in year-to-year variations in the

simulated current fields (Fig. 8 and Fig. 9), and thereby influence the simulated speed and pathway of the tracers. For instance, the spreading of the Sellafield signal in the Arctic Ocean in this study is quite different from that in [Nies et al., 1998]. In the latter study, peak values of the Sellafield signal were obtained in 1985 and 1990 at the North Pole, whereas mainly found on the Atlantic side of the Pole in this study (Fig. 5). It is hard to assess which model realisation is the most realistic. It is well known, however, that the sea ice and surface water circulation in the Arctic Ocean are highly determined by the natural variability modes of the atmospheric circulation, notably the NAO and the closely associated Arctic Oscillation (AO; [Mysak, 2001]). It is therefore of particular importance to use realistic atmospheric forcing fields when simulating transport and mixing of tracers in the Arctic Ocean.

The synoptic-forced integration presented here shows some of the features that can be deduced from an OGCM tracer simulation. It is, as an example, interesting to note that in the AW off the coast of Norway, the atmospheric fallout of ^{137}Cs and ^{90}Sr dominates over the Sellafield release from the early 1990s and onwards (see Fig. 7f,g). The degree of realism of this finding highly depends on the quality of the simulated transport and mixing processes, and the representativeness of the applied time history of the Sellafield release and the atmospheric fallout. It is also interesting to note how the radionuclides signal first builds up and thereafter diminishes in the Nordic Seas–Arctic Ocean region. This shift is most clearly seen in the 1980s when a substantial fraction of the radionuclides is transported southward across the Greenland–Scotland Ridge, before continuing southward in the Atlantic Ocean as a part of the geostrophically controlled Deep Western Boundary Current off the coast North America (particularly Fig. 6e–g).

Acknowledgements

References

Arakawa and Lamb, 1977. A. Arakawa and V. Lamb, Computational design of the basic processes of the UCLA General Circulation Model. *Methods Comput. Phys.* **17** (1977), pp. 174–265.

Bentsen et al., 1999. M. Bentsen, G. Evensen, H. Drange and A.D. Jenkins, Coordinate transformation on a sphere using conformal mapping. *Mon. Wea. Rev.* **127** (1999), pp. 2733–2740.

Bleck et al., 1995. R. Bleck, S. Dean, M.O. Keefe and A. Sawdey, A comparison of data-parallel and message-passing versions of the Miami Isopycnic Coordinate Ocean Model. *Parallel Comput.* **21** (1995), pp. 1695–1720.

Bleck et al., 1992. R. Bleck, C. Rooth, D. Hu and L.T. Smith, Salinity-driven thermohaline transients in a wind- and thermohaline-forced isopycnic coordinate model of the North Atlantic. *J. Phys. Oceanogr.* **22** (1992), pp. 1486–1515.

Dahlgaard, 1995. H. Dahlgaard, Transfer of European coastal pollution to the Arctic: radioactive tracers. *Mar. Pollut. Bull.* **31** (1995), pp. 3–7.

Drange and Simonsen, 1996. Drange, H., Simonsen, K., 1996. Formulation of air–sea fluxes in the ESOP2 version of MICOM. Tech. Rep. 125, Nansen Environmental and Remote Sensing Center, Edv. Griegsv. 3A, N-5059 Solheimsviken, Norway.

England and Holloway, 1998. M. England and G. Holloway, Simulations of CFC content and water mass age in the deep North Atlantic. *J. Geophys. Res.* **103** C8 (1998), pp. 15885–15901.

England and Maier-Reimer, 2001. M. England and E. Maier-Reimer, Using chemical tracers to assess ocean models. *Rev. Geophys.* **39** 1 (2001), pp. 29–70.

Friedrich and Levitus, 1972. H. Friedrich and S. Levitus, An approximation to the equation of state for sea water, suitable for numerical ocean models. *J. Phys. Oceanogr.* **2** (1972), pp. 514–517.

Gao et al., in press. Gao, Y., Drange, H., Bension, M., 2003. Effects of diapycnal and isopycnal mixing on the ventilation of CFCs in the North Atlantic in an isopycnic coordinate OGCM. Tellus, in press.

Gargett, 1984. A. Gargett, Vertical eddy in the ocean interior. *J. Mar. Res.* **42** 2 (1984), pp. 359–393.

Gaspar, 1988. P. Gaspar, Modeling the seasonal cycle of the upper ocean. *J. Phys. Oceanogr.* **18** (1988), pp. 161–180.

Hansen and Østerhus, 2000. B. Hansen and S. Østerhus, North Atlantic–Nordic Seas exchanges. *Prog. Oceanogr.* **45** 2 (2000), pp. 109–208.

Harder, 1996. Harder, M., 1996. Dynamik, Rauhigkeit und Alter des Meereises in der Arktis. Ph.D. Thesis, Alfred-Wegner-Institut für Polar- ind Meeresforschung, Bremerhaven, Germany.

Hibler, 1979. W. Hibler, A dynamic thermodynamic sea ice model. *J. Phys. Oceanogr.* **9** (1979), pp. 815–846.

Hurrell, 1995. W. Hurrell, Decadal trends in the north Atlantic oscillation: regional temperatures and precipitation. *Science* **269** (1995), pp. 676–679.

Ingvaldsen et al., 2002. R. Ingvaldsen, H. Loeng and L. Asplin, Variability in the Atlantic inflow to the Barents Sea based on a one-year time series from moored current meters. *Cont. Shelf Res.* **22** (2002), pp. 505–519.

Kalnay et al., 1996. E. Kalnay, M. Kanamitsu, R. Kistler, W. Collins, D. Deaven, L. Gandin, M. Iredell, S. Saha, G. White, J. Woollen, Y. Zhu, M. Chelliah, W. Ebisuzaki, W. Higgins, J. Janowiak, K.C. Mo, C.

Ropelewski, J. Wang, A. Leetmaa, R. Reynolds, R. Jenne and D. Joseph, The NCEP/NCAR 40-year reanalysis project. *Bull. Amer. Meteor. Soc.* **77** 3 (1996), pp. 437–471.

Kershaw and Baxter, 1995. P. Kershaw and A. Baxter, The transfer of reprocessing wastes from northwest Europe to the Arctic. *Deep Sea Res.* **42** (1995), pp. 1413–1448.

Levitus and Boyer, 1994. Levitus, S., Boyer, T.P., 1994. World Ocean Atlas 1994 Volume 4: Temperature. NOAA Atlas NESDIS 4. Washington, DC, USA.

Levitus et al., 1994. Levitus, S., Burgett, R., Boyer, T.P., 1994. World Ocean Atlas 1994 Volume 3: Salinity. NOAA Atlas NESDIS 3. Washington, DC, USA.

Livingston et al., 1984. H. Livingston, S. Kupferman, V. Bowen and R. Moore, Vertical profile of artificial radionuclide concentrations in the central Arctic Ocean. *Geichimica et Cosmochimica Acta* **48** (1984), pp. 2195–2203.

McDougall and Dewar, 1998. T. McDougall and W. Dewar, Vertical mixing, cabbeling and thermobaricity in layered models. *J. Phys. Oceanogr.* (1998), pp. 1458–1480.

Mysak, 2001. L.A. Mysak, Patterns of Arctic circulation. *Science* **293** (2001), pp. 1269–1270.

Nies et al., 1998. H. Nies, H. Harms, M. Karcher, D. Dethleff, C. Bahe, G. Kuhlmann, J. Oberhuber, J. Backhaus, E. Kleine, P. Loewe, D. Matishov, A. Stepanov and O. Vasiliev, Anthropogenic radioactivity in the Nordic Seas and the Arctic Ocean—results of a joint project. *Deutsche Hydrographische Zeitschrift* **50** 4 (1998), pp. 313–343.

Nilsen et al., in press. Nilsen, J.E.Ø., Gao, Y., Drange, H., Furevik, T., Bentsen, M., 2003. Simulated North Atlantic–Nordic Seas water mass exchanges in an isopycnic coordinate OGCM. Geophys. Res. Lett., 30.

Smolarkiewicz and Clark, 1986. P.K. Smolarkiewicz and T.L. Clark, The multidimensional positive definite advection transport algorithm: further development and applications. *J. Comp. Phys.* **67** (1986), pp. 396–438.

Strand et al., 1996. P. Strand, A. Aarkrog, J. Bewers, Z. Tsaturov and S. Magnusson, Radioactive contamination of the Arctic marine environment. In: *Radionuclides in the Oceans—Inputs and Inventories*, Inst. de Protection et de Surete Nucleaire, France (1996), pp. 95–119.

Strand et al., 1998. Strand, P., Balonov, M., Aarkrog, A., Bewers, M.J., Howard, B., Salo, A., Tsaturov, Y.S., 1998. Radioactivity. In: AMAP (Ed.), AMAP Assessment Report: Arctic Pollution Issues. Arctic Monitoring and Assessment Programme (AMAP), Oslo, Norway, p. 859.

Toggweiler et al., 1989. J. Toggweiler, K. Dixon and K. Bryan, Simulations of radiocarbon in a coarse-resolution world ocean model, 1, Steady state prebomb distributions. *J. Geophys. Res.* **94** (1989), pp. 8217–8242.

Turrell et al., 2002. Turrell, W.R., Hansen, B., Hughes, S., Østerhus, S., 2002. Hydrographic variability

during the decade of the 1990s in the Northeast Atlantic and southern Norwegian Sea. ICES Symposium on Hydrobiological Variability in the ICES Area, 1990–99. ICES Mar. Sci. Symp., ICES.

UNSCEAR, 1982. UNSCEAR, 1982. Ionizing radiation: sources and biological effects. UNSCEAR 1982 Report to the General Assembly with Scientific Annexes. United Nations Scientific Committee on the Effects of Atomic Radiation, United Nations, New York.

Visbeck et al., in press. Visbeck, M., Chassignet, R., Delworth, T., Dickson, B., Krahmann, G., 2002. The ocean's response to North Atlantic oscillation variability. In: Hurrell, J., Kushnir, Y., Ottersen, G., Visbeck, M. (Eds.), The North Atlantic Oscillation. AGU monograph, in press.

Zalesak, 1979. S. Zalesak, Fully multidimensional flux-corrected transport algorithms for fluids. *J. Comp. Phys.* **31** (1979), pp. 335–362.